

Carrier-Confined Vertical-Cavity Semiconductor Optical Amplifiers for Higher Gain and Efficiency

E. Staffan Björilin, *Member, IEEE*, Toshio Kimura, and John E. Bowers, *Fellow, IEEE*

Abstract—Vertical-cavity semiconductor optical amplifiers (VCSOAs) are interesting devices because of their small form factor, potential low manufacturing cost, high coupling efficiency to optical fiber, and polarization-independent gain. In this paper, we present an overview of the properties of VCSOAs, as well as emerging applications for this new class of devices. We present general design rules and analyze how the mirror reflectivity affects the properties of the VCSOA. Experimental results of carrier-confined, optically pumped VCSOAs operating at 1.3- μm wavelength are presented. The devices were fabricated by wafer bonding high-quality AlGaAs distributed Bragg reflectors (DBRs) to an InGaAsP/InP active region. A carrier-confining structure was formed on the active region *before* the top mirror was bonded to the sample. These VCSOAs show the highest fiber-to-fiber gain (17 dB) and the lowest noise figure (6.1 dB) of any long-wavelength VCSOAs to date. VCSOAs should find applications as low-cost, single-channel amplifiers, amplifying filters, amplifying switches or modulators, as well as in two-dimensional array applications such as optical interconnects. We demonstrate the use of VCSOAs for optical preamplification at 10 Gb/s. Using an 11-dB gain VCSOA, the sensitivity of a regular p-i-n detector was increased by 7 dB resulting in a receiver sensitivity of -26.2 dBm.

Index Terms—Fabry–Perot (FP) resonators, laser amplifiers, optical filters, optical resonators, semiconductor optical amplifiers, surface-emitting lasers, vertical-cavity devices, vertical-cavity semiconductor optical amplifiers (VCSOAs).

I. INTRODUCTION

THERE is currently significant interest in amplifier technologies that can provide a cost-effective alternative to erbium-doped fiber amplifiers (EDFAs). Potential low-cost technologies such as erbium-doped waveguide amplifiers (EDWAs) and semiconductor optical amplifiers (SOAs) are being pursued by several companies. An alternative to the conventional in-plane SOAs are vertical-cavity semiconductor optical amplifiers (VCSOAs). The vertical-cavity design gives VCSOAs a number of advantages over in-plane devices, such as high coupling efficiency to optical fiber, small form factor, low power consumption, and the possibility of fabricating two-dimensional (2-D) arrays on wafer. Furthermore, the technology allows for on-wafer testing and is compatible with low-cost manufacturing and packaging techniques. These advantages all draw from the fundamental geometrical differences between

the vertical-cavity and the in-plane designs. In a vertical-cavity structure, the optical mode passes perpendicularly through the different material layers. Consequently, the optical field is always parallel to the active layers, which makes it easier to obtain polarization-independent gain. It also makes the gain per pass very small, on the order of a few percent. VCSOAs therefore use feedback provided by high reflectivity distributed Bragg reflector (DBR) mirrors. The feedback constricts the gain bandwidth to the linewidth of the Fabry–Perot (FP) mode, which essentially limits the operation to amplification of a single signal. The narrow bandwidth also filters out out-of-band noise, making VCSOAs ideal as preamplifiers in receiver modules. The vertical cavity is circular symmetric around the axis perpendicular to the two mirrors and naturally supports a circular optical mode. This yields high coupling efficiency to optical fiber, which is beneficial for achieving a low noise figure.

Remarkably little work has been done on VCSOAs. The first SOA was presented in 1963 [1] and the first vertical-cavity surface-emitting laser (VCSEL) in 1979 [2]. Since then, extensive work has been done on both types of devices but the combination—VCSOAs—have attracted little interest. In 1991, the first VCSOA was demonstrated by the same research group at Tokyo Institute of Technology that presented the first VCSEL. Koyama, Kubota, and Iga [3] used an electrically pumped GaAs/AlGaAs VCSEL structure to amplify and filter an injected 885-nm signal. The input signal was injected through the bottom mirror, which consisted of seven periods $\text{SiO}_2/\text{TiO}_2$. The output (top) mirror consisted of $\text{Au}/\text{SiO}_2/\text{TiO}_2/\text{SiO}_2$. The favorable filtering properties stemming from the high-finesse VCSEL cavity was recognized; the device was not presented as an amplifier but as an active filter. No fiber-to-fiber gain was obtained but about 4-dB internal gain was reported.

Two years later, in 1993, an optically pumped reflection mode device, also at 850 nm, was presented by Raj *et al.* at France Telecom. It was presented as an amplifying photonic switch. Only pulsed operation was reported [4]. The same group introduced resonant pumping in a following generation of 850-nm devices [5] and in 1996 they presented the first long-wavelength VCSOA [6]. The device was again presented as an amplifying switch. It was optically pumped and operated in reflection mode. The operating wavelength was 1.55 μm . The sample consisted of an InP/InGaAs active region with two sets of five quantum wells (QWs), a gold-bottom mirror, and a two period Si– SiO_2 top mirror. 14 dB of gain was achieved in pulsed operation. Also in 1996, Wiedenmann *et al.* at the University of Ulm presented an electrically pumped reflection mode VCSOA operating at 980 nm [7]. In 1998, they presented

Manuscript received February 14, 2003; revised July 24, 2003. The VCSOA project at University of California, Santa Barbara is supported by the Defense Advanced research Projects Agency (DARPA) via the Center for Chips with Heterogeneously Integrated Photonics (CHIPS).

The authors are with the Department of Electrical and Computer Engineering, University of California, Santa Barbara, Santa Barbara, CA 93106 USA (e-mail: bjorlin@ece.ucsb.edu).

Digital Object Identifier 10.1109/JSTQE.2003.819480

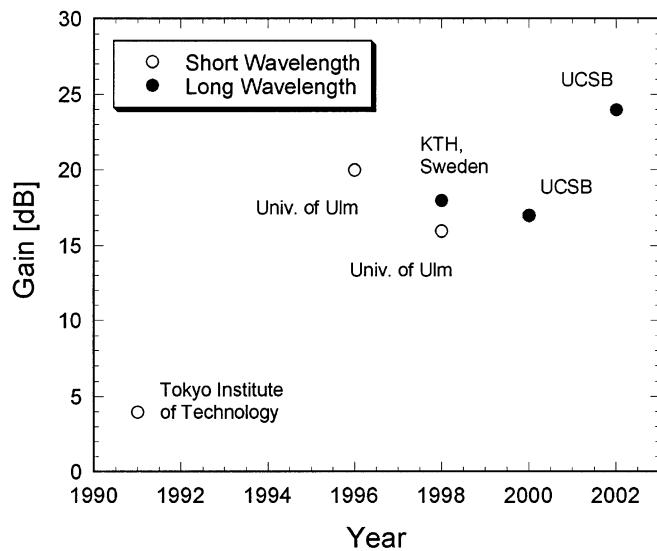


Fig. 1. Progress in amplifier gain of VCOSAs.

their second generation of devices: an electrically pumped, transmission-mode VCOSA with an oxide aperture for current and mode confinement [8]. Whereas many VCOSAs before this were either merely VCSELs operated below threshold or very simple designs that required complicated experimental setups and pumping schemes, what Wiedenmann *et al.* presented was a very practical device because of the electrical pumping and transmission mode operation. They achieved 16 dB of gain. However, the operating wavelength was 980 nm, which is not very interesting for telecomm applications. In 1998, Lewen *et al.* at the Royal Institute of Technology (KTH) in Sweden used a 1.55- μm VCSEL structure for what was the first electrically pumped long-wavelength VCOSA [9]. The device had an InP/InGaAsP bottom DBR and a Si/SiO₂ top DBR. They measured 18 dB of gain at 218 K not including coupling losses; the fiber-to-fiber gain was not quoted. The device saturated very early (less than -25 -dBm saturated output power) and the bandwidth was extremely narrow, most likely because the device was optimized as a VCSEL, not an amplifier. The VCOSA project at the University of California, Santa Barbara (UCSB) started in 1999 and led to the demonstration of the first 1.3- μm VCOSA in 2000 [10]. These devices were fabricated using InP-GaAs wafer bonding, they were optically pumped, and operated in reflection mode. This first generation was used to fully characterize this still fairly new class of devices [11], [12], to develop improved theoretical models [13], [14], and to explore possible applications for VCOSAs [15], [16]. A second generation of 1.3- μm devices with improved efficiency and record high gain was recently presented [17]. The progress in continuous wave (CW) amplifier gain of VCOSAs (not including coupling losses) is summarized in Fig. 1.

In this paper, we overview the design, characteristics, and possible applications of VCOSAs. In Section II, a broad theoretical VCOSA model is presented. The model is used to derive a few useful design rules in Section III. The effect that the reflectivity of the mirrors has on the VCOSA properties is analyzed,

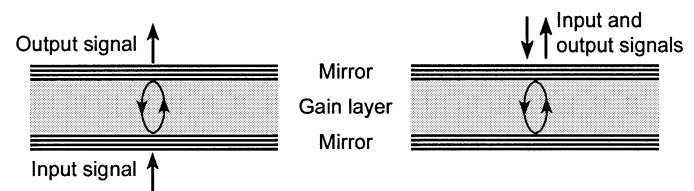


Fig. 2. Schematic of VCOSAs showing transmission mode operation (left) and reflection mode operation (right).

and different designs are discussed. In Section IV, our most recent long-wavelength VCOSA's results are presented. Potential applications for VCOSAs are discussed in Section V, including the demonstration of optical preamplification at 10 Gb/s.

II. THEORETICAL MODEL

The basic structure of a VCOSA consists of an active region enclosed by two mirrors. The device can be optimized for operation in either the reflection or transmission mode, as shown schematically in Fig. 2. In the reflection-mode operation, the signal is injected and collected from the top, through the top mirror. A bottom mirror reflectivity close to unity is desired, and the top mirror reflectivity can be varied to change the properties of the VCOSA. In the transmission-mode operation both mirrors are slightly transmissive. The signal is injected through one side and collected on the other side.

The first theoretical predictions of VCOSA performance was presented by Tombling *et al.* in 1994 [18]. The model that was used was based on carrier and photon rate equations and the FP equations for a cavity with gain. Karlsson *et al.* used a similar approach, but also analyzed the detector characteristics of VCOSAs in a 1996 publication [19]. In 1999, Kibar presented a detailed VCOSA analysis based on small-signal equivalent circuits and rate equations [20]. In 2000, Piprek *et al.* presented a more detailed rate equation model [13]. Of these publications, only Tombling *et al.* [18] analyzed all four important amplifier parameters (gain, gain bandwidth, saturation, and noise figure). However, no experimental results were presented to validate their theoretical model. More importantly, in these early theoretical VCOSA papers—as well as in even older in-plane SOA publications—the results obtained using rate equation analysis and the FP approach did not agree. This disagreement was caused by the omission of interference between the fields that traverse the input mirror in both directions. This omission led to an incorrect expression for the mirror loss in the photon rate equation. The problem was solved in 2002 by Royo *et al.* who showed that the mirror loss actually depends on the gain in the amplifier [21].

The well-known FP equations for a cavity with gain [22] are a convenient tool to model the gain spectrum of VCOSA. In this model, the DBRs are replaced by hard mirrors separated by an effective cavity length, which includes the penetration of the optical field into the mirrors. An incoming optical field is considered and all field components exiting the cavity are added together to get the output field. To obtain the power gain, the

fields are squared and the total output power is divided by the input power. The gain for transmission mode (G_t) and reflection mode (G_r) operation are given by

$$G_t = \frac{(1 - R_t)(1 - R_b)g_s}{(1 - \sqrt{R_t R_b}g_s)^2 + 4\sqrt{R_t R_b}g_s \sin^2 \phi} \quad (1)$$

$$G_r = \frac{(\sqrt{R_t} - \sqrt{R_b}g_s)^2 + 4\sqrt{R_t R_b}g_s \sin^2 \phi}{(1 - \sqrt{R_t R_b}g_s)^2 + 4\sqrt{R_t R_b}g_s \sin^2 \phi} \quad (2)$$

where R_t is the top mirror reflectivity, R_b is the bottom mirror reflectivity, g_s is the single pass gain, and ϕ is the round-trip phase detuning normalized to the cavity resonance. Note that the gain of a transmission mode device is independent of the direction of signal propagation through the device. If ϕ is set equal to zero, (1) and (2) can be used to calculate the peak gain. From (1) and (2), expressions for calculating the bandwidth are readily obtained. The gain bandwidth (full-width at half-maximum—FWHM) for the two cases are given by

$$\Delta f_t = \frac{c}{\pi n L} \cdot \arcsin \left[\frac{(1 - \sqrt{R_t R_b}g_s)^2}{4\sqrt{R_t R_b}g_s} \right]^{\frac{1}{2}} \quad (3)$$

$$\Delta f_r = \frac{c}{\pi n L} \cdot \arcsin \left[4\sqrt{R_t R_b}g_s \left(\frac{1}{(1 - \sqrt{R_t R_b}g_s)^2} - \frac{2}{(\sqrt{R_t} - \sqrt{R_b})^2} \right) \right]^{-\frac{1}{2}} \quad (4)$$

where n is the refractive index of the cavity, L is the effective cavity length, and c is the velocity of light in vacuum.

Rate equations are used to model the interaction between photons and carriers in the amplifier cavity. Compared to the well-known rate equations commonly used to analyze lasers, the rate equations for amplifiers have an additional term for the input signal. Furthermore, the mirror loss has to be modified as mentioned above. The rate equations for carriers (N) and photons (S) then take the following form:

$$\frac{dN}{dt} = G_{\text{gen}} - \Gamma_{\text{enh}}v_g g S - (AN + BN^2 + CN^3) \quad (5)$$

$$\frac{dS}{dt} = \frac{\eta P_s}{h\nu V} + \beta \Gamma BN^2 + \Gamma_{\text{enh}}\Gamma v_g g S - (\alpha_i + \alpha_m)v_g S. \quad (6)$$

The first term on the right-hand side of (5), G_{gen} is a carrier-generation term that is different depending on whether electrical or optical pumping is used. The second term is the stimulated recombination and the last term summarizes all recombination processes that do not contribute to amplification of the signal. Γ_{enh} is the gain enhancement factor, v_g is the group velocity, and g is the material gain. AN is the defect recombination, BN^2 is the spontaneous emission, and CN^3 is Auger recombination. The first term on the right-hand side of (6) describes the injection of the input signal into the cavity. The second term is the spontaneous recombination, the third term the stimulated recombination, and the last term is the loss of photons. η is the coupling efficiency into the VCSEA, P_s is the input signal power, $h\nu$ is the energy per signal photon, V is the active volume, β is the spontaneous emission coefficient, Γ is the confinement factor, α_i is the average cavity loss, and α_m is the

mirror loss, which depends on the amplifier gain. The mirror loss is calculated using [21]

$$\alpha_m = \frac{1}{L} \left(\frac{G_r + G_t}{G_r + G_t - 1} \right) \cdot \ln g_s. \quad (7)$$

The rate equations contain a large number of unknown material and design specific parameters. In order to obtain reliable results, as accurate values as possible have to be found for these unknown parameters. The FP equations also contain a few unknowns, albeit fewer than the rate equations. The results obtained using the FP equations are therefore more general. The calculations presented in the next section are based on the design of the devices presented in Section IV and a gain model calculated using an advanced laser simulation software, as described in [13]. The rate equations were fitted to measured gain saturation data in order to find viable values for the unknown parameters. The coupling efficiency of pump light into the VCSEA, and the defect recombination were used as fitting parameters. The aim of this paper is to show general trends; all details of the theoretical model outlined above can be found in [23].

III. VCSEA DESIGN

A. Gain and Gain Bandwidth

The model described above can now be used to calculate how properties of VCSEAs vary with changes in some key design parameters. The balance between gain and reflectivity is central in VCSEA design. By plotting the amplifier gain versus mirror reflectivity for different values of single-pass gain, and for operation as close to threshold as desired, the best operating point for a given active region design can be found. Fig. 3 shows gain (bottom) and gain bandwidth (top) versus mirror reflectivity for a transmission mode VCSEA. One mirror reflectivity is held constant at 0.95 and the reflectivity of the other mirror is represented on the x -axis. It is assumed that the maximum single-pass gain that can be reached is 8%. This assumption is based on the design of the active region of the VCSEAs presented later in this paper, which had 21 InAs_{0.5}P_{0.5} QWs. Four pairs of curves representing constant single-pass gains of 2%, 4%, 6%, and 8% are shown. These curves were calculated using (1) and (3). The FP model is only valid below lasing threshold, which is given by the condition $g_s R_1 R_2 = 1$. The signal gain goes toward infinity and the gain bandwidth goes to zero at lasing threshold. Also shown are gain curves at 95% and 90% of the pump power required to reach lasing threshold. Those curves were calculated using the rate equations. The curve corresponding to a single-pass gain of 8%, together with the 95% of threshold curve, mark the maximum amplifier gain that can be obtained. These curves are shown as solid lines. The point at which they cross represents the optimum mirror reflectivity and the highest possible amplifier gain. For the case of transmission-mode operation and the active region used here, the optimum reflectivity is 0.9, which gives a gain of about 30 dB. To the left of this point, the maximum gain is limited by the maximum material gain (in this case assumed to be 3500 cm⁻¹). Lasing threshold cannot be reached, and the active region can be pumped to full population inversion for low-noise performance. To the right of the crossing point, the VCSEA performance is limited by lasing threshold. The dashed curves show performance trends for lower values of single-pass

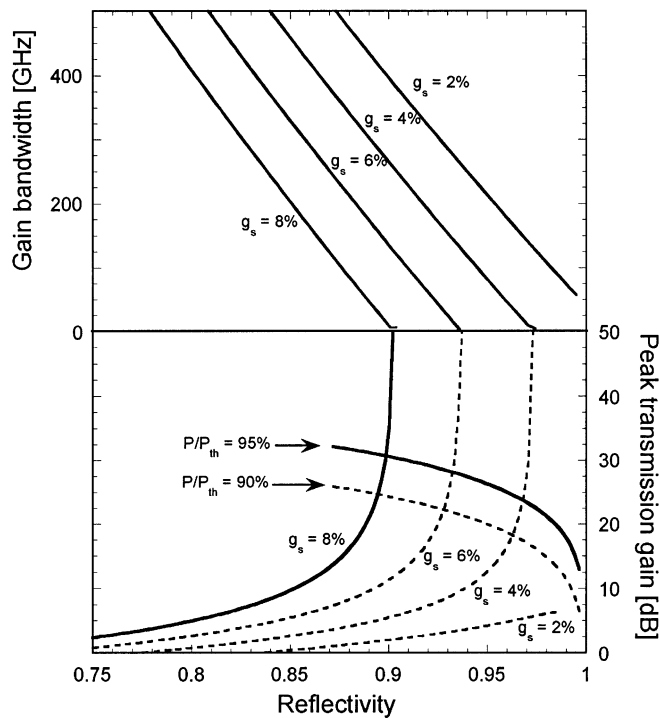


Fig. 3. Peak gain and gain bandwidth versus mirror reflectivity for transmission mode operation. The reflectivity of one mirror is held constant at 0.95. The solid lines in the bottom half of the figure indicate maximum achievable gain. The dashed curves indicate trends.

gain and operation further away from lasing threshold. The gain curves for constant single-pass gain are the most general as they only need three input parameters— R_t , R_b , and g_s . The bandwidth curves are not as general as they require values for the length and refractive index of the cavity. The curves calculated using the rate equations are the least general as they involve a number of design-specific parameters. Fig. 4 shows gain and gain bandwidth versus top mirror reflectivity for the case of reflection mode operation. For this case, the bottom mirror reflectivity is 0.999. Optimum mirror reflectivity and highest possible gain as suggested by the graph are in this case about 0.85 and 35 dB. The single-pass gain needed to achieve high amplifier gain is higher for transmission-mode operation because of the higher combined mirror loss.

Figs. 3 and 4 give the impression of a tradeoff between gain and bandwidth. However, this is only true for a constant single-pass gain, such as the maximum gain in the low-reflectivity regime. In the high-reflectivity regime, where the performance is limited by lasing threshold, decreased reflectivity allows for stronger pumping and thereby higher gain. Because of this tradeoff, the gain–bandwidth product is a good figure of merit for VCISOAs. It is defined as the square root of the gain times the bandwidth. It can be shown that the gain–bandwidth product increases with decreased mirror reflectivity for both transmission and reflection mode operation [14].

B. Saturation Power

As the photon density in the cavity is increased, the gain medium eventually saturates and the gain drops. This occurs

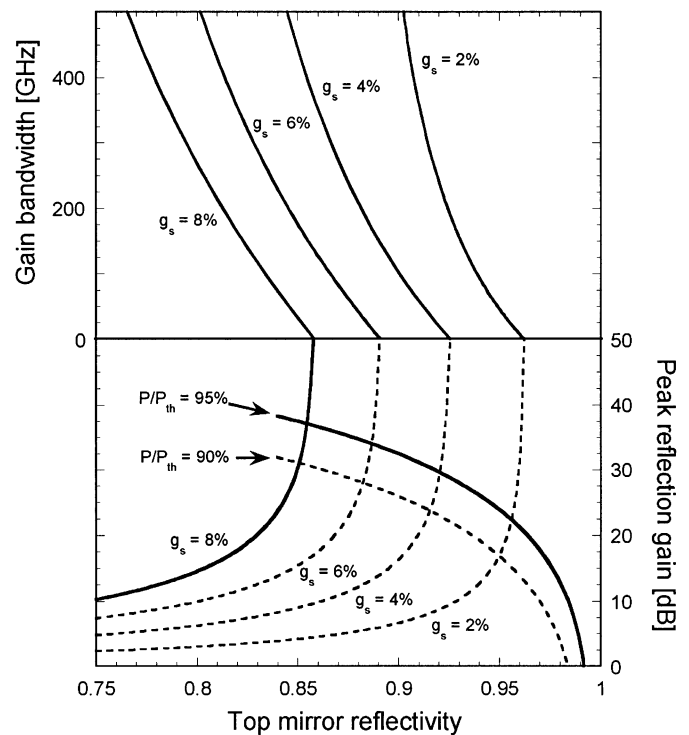


Fig. 4. Peak gain and gain bandwidth versus top mirror reflectivity for reflection mode operation. The bottom mirror reflectivity is 0.999.

when the signal power is increased or when the VCISOA is operated close to threshold in which case the amplified spontaneous emission (ASE) causes gain saturation. The saturation input power is defined as the input signal power for which the gain drops by 3 dB from its small-signal value. The saturation properties of the VCISOA can be modeled using the rate equation approach. For high saturation power (and high output power) it is clearly desirable to maintain a large carrier density to photon density ratio as the signal power is increased. This can be achieved by making the active volume large and reduce the photon cavity lifetime (lower photon density) and pump the device hard (high carrier density). The drawback is that high gain in a large active volume leads to higher power consumption. Saturation input power versus unsaturated gain for transmission- and reflection-mode operation are shown in Figs. 5 and 6, respectively. As the pump power is increased, the gain increases due to the increased carrier density. The increase in gain results in increased photon density. This causes the gain to saturate earlier, except for the case of high gain at very low mirror reflectivities. Depending on the slope of the curve, the saturation *output* power may decrease, stay constant, or increase. This varies along the curves, but depends on the specific VCISOA design as well.

C. Noise Figure

The noise figure of an optical amplifier describes the signal-to-noise ratio (SNR) degradation as a signal passes through the amplifier. This makes the noise figure one of the most important properties of optical amplifiers for their applications in optical communication systems. The noise figure of VCISOAs can be analyzed using the same methods

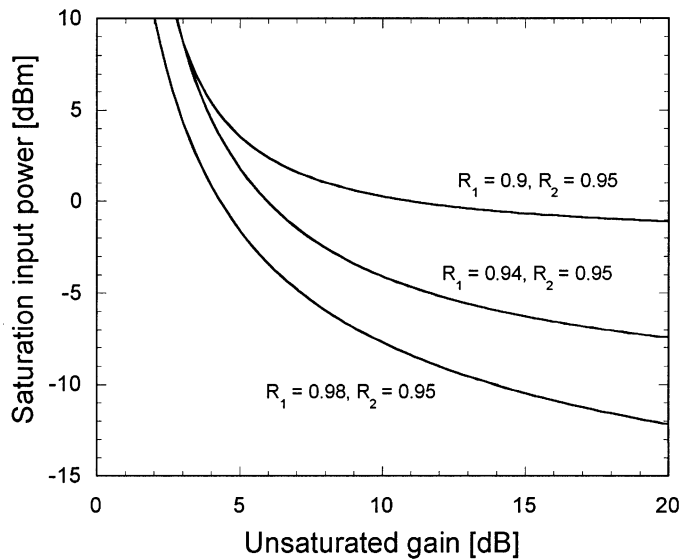


Fig. 5. Saturation input power versus unsaturated gain for transmission-mode operation.

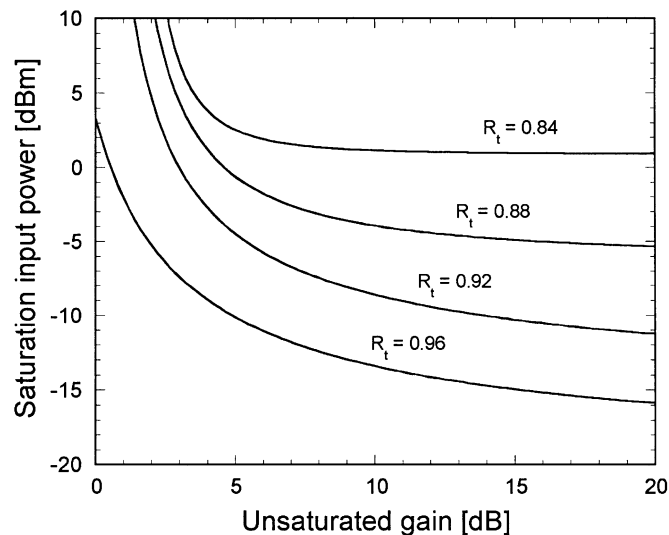


Fig. 6. Saturation input power versus unsaturated gain for reflection mode operation. The bottom mirror reflectivity is 0.999.

as for in-plane FP amplifiers [24]. The total output noise from an optical amplifier consists of several different noise terms of different origin. The terms contributing to the total noise are: beating between ASE components and the coherent signal light, beating between different ASE components, and shot noise due to both signal and ASE. The input signal might also have some excess noise and the receiver adds thermal noise. Spontaneous-spontaneous beat noise is independent of the input signal power and is the dominating term at low-signal power. This term depends on the optical bandwidth of the ASE spectrum. For this reason, a bandpass filter is normally used after the optical amplifier in order to minimize the amount of ASE reaching the detector. This is not needed for a VCISOA as the spontaneous emission bandwidth is limited by the FP cavity. Signal-spontaneous beat noise and shot noise increase with input-signal power. At high signal powers, signal-spontaneous

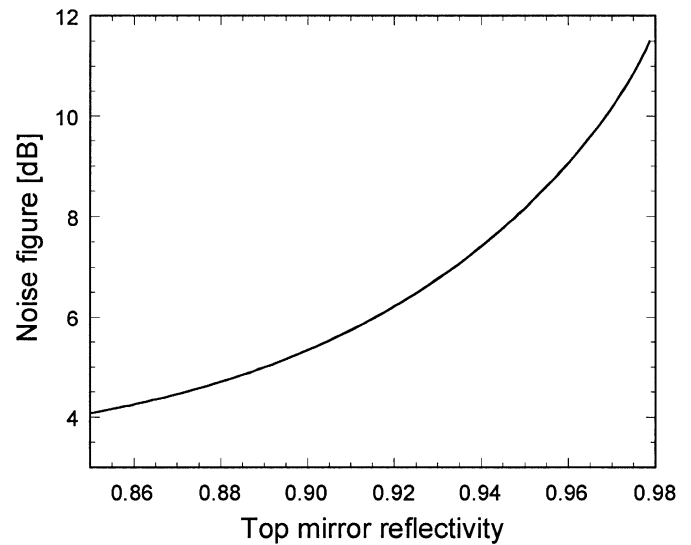


Fig. 7. Calculated noise figure at $P/P_{th} = 0.9$ versus top mirror reflectivity for the devices presented later in this paper.

beat noise is the main contributor to the output noise. The output ASE, and hence the signal-spontaneous beat noise is greatly affected by the mirror reflectivity.

Considering signal-spontaneous beat noise to be dominant, the noise factor F , defined as input SNR over output SNR (the noise figure is defined as $NF = 10 \log(F)$ and expressed in decibels), is given by $F = 2n_{sp}\chi(G-1)/G$, which for high signal gain ($G \gg 1$) reduces to $F = 2n_{sp}\chi$. Here, n_{sp} is the population inversion parameter and χ is the excess noise coefficient, which describes signal-spontaneous beat noise enhancement due to finite mirror reflectivity. χ takes a value of one for zero reflectivity (the case of traveling-wave amplifiers) and values higher than one for finite mirror reflectivities. An excess coefficient of one can be obtained for VCISOAs if the mirror reflectivities are chosen properly [12]. For a reflection mode device, χ depends only on the bottom mirror reflectivity, which should be as high as possible. A bottom mirror reflectivity over 0.999, which is easily obtained using DBR mirrors, yields $\chi \approx 1$. For the case of transmission-mode operation, low-input mirror reflectivity is desired in order to minimize χ . The population inversion parameter n_{sp} equals one for complete inversion and higher values for incomplete inversion. It is desired to operate at as high carrier density as possible in order to minimize n_{sp} . A problem inherent to FP amplifiers is that the strong pumping needed to minimize n_{sp} could result in lasing if the mirror reflectivity is too high. It is, therefore, of utmost importance that the mirror reflectivities are low enough to allow full inversion without the onset of lasing. Fig. 7 shows calculated noise figure at 90% of threshold versus mirror reflectivity ($R_t \times R_b$) for the devices presented later in this paper. An excess noise coefficient of one was used in the calculation. Only signal-spontaneous beat noise is included in the calculation because it dominates over spontaneous-spontaneous beat noise by at least one order of magnitude for input signal power over -45 dBm. A noise figure of about 4 dB can be expected for a reflectivity of 0.85. For any practical application, the critical parameter is not the intrinsic noise figure of a device but rather

its fiber-to-fiber noise figure. The noise figure is degraded by loss associated with coupling of the signal into the VC SOA (in logarithmic units, the input coupling loss is simply added to the noise figure). VC SOAs have superior coupling efficiency compared to in-plane devices and can therefore be expected to show better fiber-to-fiber noise figures.

To summarize the theory trends, strong feedback, i.e., high mirror reflectivity, leads to high gain for a given value of single-pass gain, but the gain is limited by a lasing threshold. It also leads to poor noise figure and early saturation. Central to the design of VC SOAs is the balance between the gain provided by the active region and the reflectivity of the two mirrors. For optimum performance, it is desirable to use mirror reflectivities that are high enough to yield high signal gain, but low enough to allow operation at high carrier density without lasing to occur. This condition gives the highest possible amplifier gain and gain-bandwidth product, the highest saturation output power, and the lowest noise figure. It is easier to achieve good amplifier characteristics in devices optimized for reflection-mode operation. The combined mirror loss is lower compared to transmission-mode operation, so good signal gain can be achieved for lower single-pass gain. Reflection-mode operation might also be a more cost-effective approach since the fiber alignment, which is a very difficult and costly step in the manufacturing, is reduced from two fibers to one. However, the input and output signals need to be separated. The separation calls for an additional component (coupler or circulator), which adds complexity, cost, and signal loss. Operation in transmission mode is more attractive in some applications, e.g., integration with detectors for preamplification or array applications. It is, however, a more difficult approach as far as testing and packaging. The choice of operational mode might ultimately depend on the intended application for the VC SOA.

D. Active Region Design

The development of VC SOAs has benefited greatly from VCSEL research over the past decade. Materials and processing technologies developed for VCSELs can be directly applied to VC SOAs, and the design of the two is in many ways similar. The main difference is that strong feedback is desired for VCSELs in order to minimize the required threshold current. In VC SOAs, on the other hand, reduced feedback is advantageous in order to enable high gain without the onset of lasing. Therefore, VC SOAs require higher single-pass gain and lower mirror reflectivity than VCSELs. The different VC SOAs presented over the past decade have shown great diversity in design and materials. Some have been optimized as amplifiers; some were merely VCSELs operated below threshold. Some structures were all-epitaxial, some used deposited insulating DBRs, and some used wafer bonding to combine long-wavelength InP-based active regions with high-reflectivity AlGaAs DBRs. Buried active regions, ion implantation, and oxide apertures have been incorporated into the designs. Almost all of the presented devices rely on multiple quantum-well (MQW) active regions to provide the high single-pass gain needed to reach sufficient amplifier gain. Only one device, the first VC SOA [3], used a bulk active region. Several designs include a longer cavity with two or more stacked MQW active regions

that provide periodic gain that matches the standing-wave pattern in the cavity. This stacked-MQW active region design is a very attractive design to achieve the high single-pass gain needed for VC SOAs. The long-wavelength devices presented so far have all used InGaAsP-based QWs [6], [9], [10], [17]. In long-wavelength VCSELs, significant progress has been made recently using AlInGaAs QWs for 1.55- μm emission [25], GaInNAs grown on GaAs for 1.3 μm [26], and Sb-based structures [27]. AlInGaAs provide improved high-temperature performance due to its larger conduction band offset and GaInNAs has the advantage of being lattice matched to GaAs. No VC SOAs have yet been reported using these materials.

The typically large number of QWs needed to reach high gain and high saturation power makes it difficult to achieve uniform carrier distribution throughout the wells using electrical injection. Optical pumping is an attractive way to pump VC SOAs for a number of reasons. Optical pumping generates carriers in the QWs, without the need of transporting the carrier through the structure. This results in very uniform carrier distribution throughout a large number of QWs. It also allows the entire structure to be undoped, which simplifies growth and processing, and minimizes optical losses. Furthermore, optical pumping can generate uniform carrier distribution across a laterally large active region. Several high-performance long-wavelength VCSELs have been presented that use optical pumping [28], [29]. To maintain a small footprint, device and pump laser can be packaged in the same package, or even integrated into the same structure [28].

IV. FABRICATION AND EXPERIMENTAL RESULTS

Two generations of VC SOAs have been developed at UCSB. Both generations operated at 1.3- μm signal wavelength and were optically pumped by a 980-nm laser. Both generations comprised a stacked InGaAsP/InP active region wafer bonded to two $\text{Al}_{0.9}\text{Ga}_{0.1}\text{As}/\text{GaAs}$ DBRs. The active region had three sets of seven compressively strained $\text{InAs}_{0.5}\text{P}_{0.5}$ QWs surrounded by strain compensating $\text{In}_{0.8}\text{Ga}_{0.2}\text{P}$ barriers. The three sets of QWs were positioned on the three central standing-wave peaks in the $5/2-\lambda$ cavity to maximize the overlap of the optical mode and the QWs. The wafer bonded interfaces were placed at nulls in the optical field in order to minimize scattering losses at the interfaces. Details about wafer bonding are reported elsewhere [30]. Both generations of devices were designed for reflection-mode operation; the bottom DBR had 26 periods, giving a calculated reflectivity of 0.999. They were made from the same active region material to facilitate a quantitative comparison of the two designs. The first generation was a gain-guided, planar structure where the lateral dimensions of the active region were defined by the spot size of the pump laser beam. The results from these devices were in good agreement with theoretical predictions [11]. High gain (13.5 dB, fiber-to-fiber) and high saturated output power (-3.5 dBm) were obtained. However, the planar structure allowed the generated carriers to diffuse laterally in the QWs, out of the active region. This resulted in low efficiency. In order to improve the efficiency in the second-generation VC SOAs, carrier confinement was introduced. A simple way to achieve

carrier confinement is to etch mesas through the active layers of the device. However, the etched sidewalls allow carriers to recombine at surface states, which can compromise the effectiveness of the carrier confinement. The degree to which surface recombination affects the carrier density in the active region depends on the materials in the active region, the quality of the sidewall surface, and the dimensions of the etched mesa. The sidewall recombination is lower in InGaAsP/InP than in the AlGaAs/GaAs material system [31]. The surface recombination states are created by the termination of the lattice. The dry etch used to form the mesas and the subsequent surface treatment are, therefore, crucial to minimizing the number of recombination sites. The number of recombination states can be reduced by chemical passivation of the sidewalls [32] or semiconductor regrowth [33].

The processing of the second-generation VCISOAs began with bonding the active region to the bottom DBR. After bonding, the InP substrate was removed. Prior to the second bond, circular mesas were defined on the active region using reactive ion etching (RIE). The etch was stopped after the third set of QWs, leaving the bottom InP cladding intact. In addition to etching vertical mesas, the QWs were underetched. This resulted in a step-like sidewall profile where the InP cladding layers had a slightly larger diameter than the QWs. Finally, the top DBR was bonded to the active region. The second wafer bond takes place at a higher temperature than the growth temperature of the QWs. During the second bond, InP from the layers surrounding the QWs migrates to smooth the steps in the sidewalls, thereby covering the QW edges. This mass transport of InP significantly reduces sidewall recombination. In addition to the intended creation of a buried heterostructure, it is advantageous for thermal reasons to have large InP layers surrounding the QW. Any heat generated in the QWs will spread to the surrounding InP layers. A larger volume of InP is simply a more efficient heat sink. The top mirror was a 10.5 period $\text{Al}_{0.9}\text{Ga}_{0.1}\text{As}/\text{GaAs}$ DBR with a calculated reflectivity of 0.918. A schematic of the carrier-confined VCISOA structure is shown in Fig. 8. A scanning-electron micrograph (SEM) of the cross section of the finished device is shown in Fig. 9.

A 980-nm laser diode was used to pump the VCISOAs through the substrate and bottom DBR. The pump beam was focused down on the VCISOA active region using free-space optics, to a spot size of $8.8\ \mu\text{m}$. A $1.3\text{-}\mu\text{m}$ external cavity tunable laser was used as signal source. A single-mode fiber and a lens were used to inject the $1.3\text{-}\mu\text{m}$ signal through the top mirror of the device and to collect the output signal. The spot size of the signal was about $8.3\ \mu\text{m}$. The input and the output signals were separated by means of an optical circulator. The total coupling loss (including loss in the circulator) was about 7 dB. An optical spectrum analyzer was used to monitor the output signal. Alignment of the pump and signal beams to overlap with the carrier-confining mesas was critical to device performance. The pump spot diameter was $0.5\ \mu\text{m}$ larger than the signal, which gave enough alignment leeway to achieve good pump-signal overlap. The best results were obtained with VCISOAs with $9\text{-}\mu\text{m}$ diameter mesas— $0.2\ \mu\text{m}$ larger than the pump spot size.

Fiber-to-fiber gain versus pump power for a carrier-confined VCISOA with a $9\text{-}\mu\text{m}$ diameter active region is shown in Fig. 10.

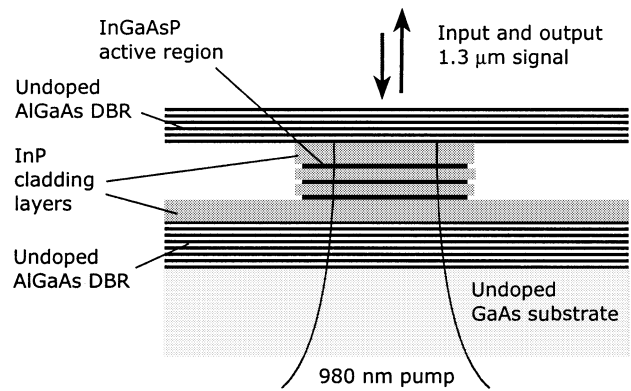


Fig. 8. Schematic of carrier-confined wafer-bonded VCISOA.

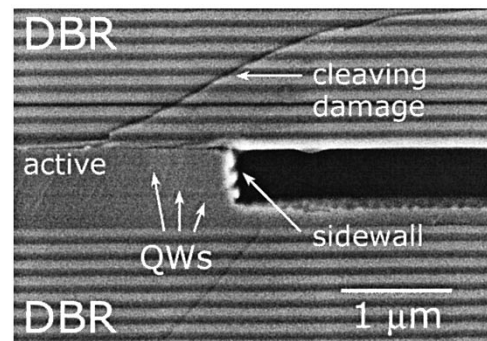


Fig. 9. SEM of cross section of carrier-confined wafer-bonded VCISOA.

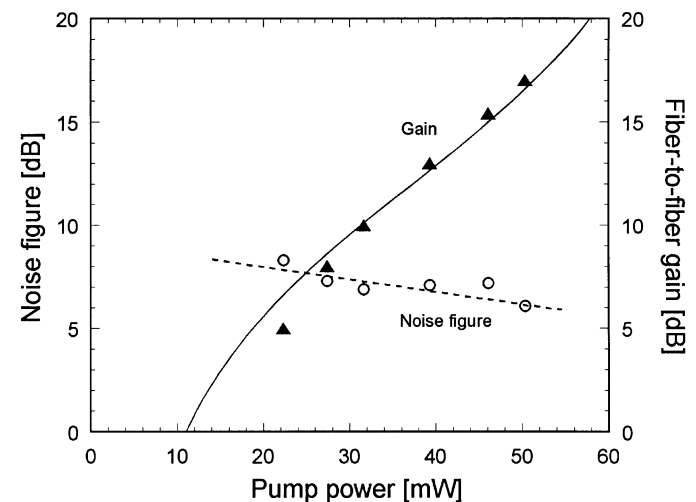


Fig. 10. Fiber-to-fiber gain and noise figure versus pump power for $9\text{-}\mu\text{m}$ diameter carrier-confined VCISOA.

Dots are measurements, the solid line is a curve fit based on the rate equations. The input signal power was $-30\ \text{dBm}$. The maximum fiber-to-fiber gain was 17 dB, measured for a pump power of 50 mW. Considering a total coupling loss of about 7 dB, the internal VCISOA gain was about 24 dB. Also shown in Fig. 10 is the fiber-to-fiber noise figure. The circles are measurements, the dashed line is a guide to the eye. For a pump power of 50 mW, a noise figure of 6.1 dB was measured. The gain spectrum of the same device is shown in Fig. 11. Dots are measurements, the line is a curve fit based on (2). The gain bandwidth for a

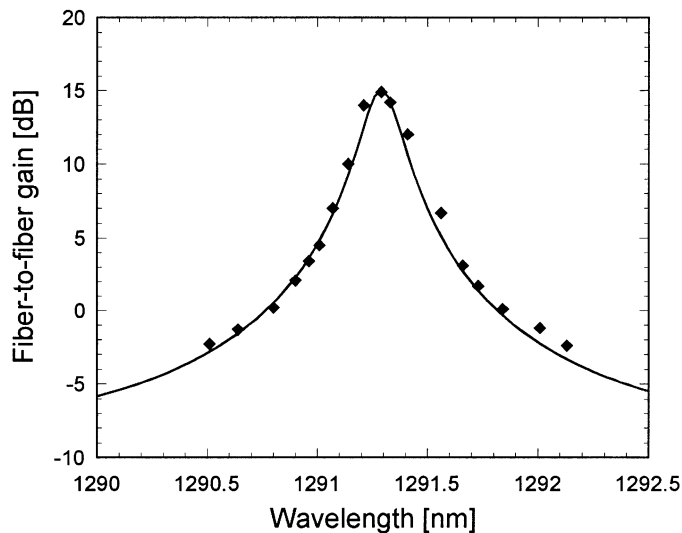


Fig. 11. Gain spectrum at 15-dB peak gain. The gain bandwidth is 0.2 nm (32 GHz).

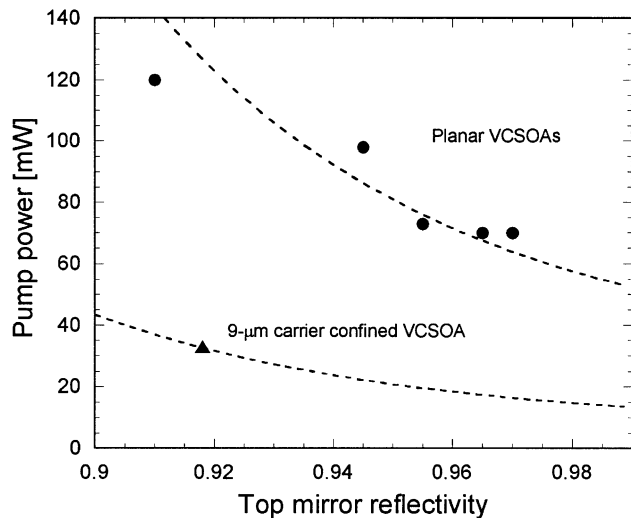


Fig. 12. Pump power required to reach 10 dB of gain for carrier-confined VCISOA compared to planar devices.

peak gain of 15 dB was measured to be 0.2 nm (32 GHz). The saturation output power for a small-signal fiber-to-fiber gain of 15.5 dB was measured to be -5 dBm. The results presented here are the best results achieved from one fabrication run. The peak signal gain of devices with the same mesa diameter, on the same sample, varied by about 3 dB. The results are in good agreement with theoretical predictions. This generation VCISOAs was designed to investigate the effect of the carrier confinement; the mesa diameter of the devices varied over a fairly wide range. No arrays of identical VCISOAs were fabricated.

Fig. 12 compares the performance of the two generations of VCISOAs. The pump power required to reach 10 dB of fiber-to-fiber gain is plotted versus top mirror reflectivity. For the planar devices, the lowest required pump power needed for 10-dB gain was about 70 mW, for devices with relatively high top mirror reflectivity. The top mirror reflectivity of the carrier-confined VCISOAs was 0.918. At that reflectivity, the planar design would

need over 100 mW of pump power to give 10-dB gain, whereas the carrier-confined design only needed 33 mW. This corresponds to a three-fold improvement in efficiency. The planar design could not be brought to lasing threshold at that reflectivity. The 9- μ m-diameter carrier-confined device lased at 60 mW of pump power. The fact that lasing threshold can be reached suggests that the QW gain is now high enough so that the top mirror reflectivity could be further reduced. This would result in higher saturation power, lower noise figure, and probably even higher amplifier gain. Unfortunately, the underetch created slightly noncircular active regions, which resulted in a small polarization-dependent gain in the smallest devices. However, this can easily be avoided through optimized processing. The three-fold improvement in efficiency and the fact that higher amplifier gain was obtained with the second-generation VCISOAs confirms that the carrier confinement had a great impact on the lateral carrier loss. The exact composition and crystalline structure of the material covering the QW edges could not be established, and the reduction in surface recombination can, therefore, not be quantified. However, the reduced carrier loss is evidence of very low sidewall recombination. This indicates that InP from the cladding layers filled in the steps in the sidewalls during the second wafer bond, effectively creating a buried heterostructure. In-plane buried heterostructure lasers fabricated by mass transport have already been demonstrated [34]. Wafer bonding provides an attractive way to fabricate buried-heterostructure VCISOAs and VCSELs, as it gives the freedom to process the active region before the structure is completed.

V. APPLICATIONS

There are a number of potential applications for VCISOAs. Compared to other amplifier technologies, the VCISOA bandwidth is very narrow and the saturation power relatively low. The noise figure of VCISOAs can be much lower than for in-plane SOAs. They can be designed to operate at any desired telecommunication wavelength. The vertical-cavity geometry is compatible with low-cost fabrication and packaging techniques. A property that is a disadvantage for one application might be the enabler of another. The narrow gain bandwidth, for instance, hinders amplification of multiple channels but provides filtering and channel selection. VCISOAs can potentially be used wherever a compact, low-cost, single-channel amplifier is needed. There are many instances in wavelength-division multiplexing (WDM) networks where the channels are split up and amplified or processed individually. A reason for this is the importance of maintaining equal signal power in all channels. VCISOAs are ideal for these applications. VCISOAs can also be integrated in high-density 2-D array architectures. This is not possible with in-plane SOAs or fiber amplifiers. It is interesting to note that in most of the VCISOAs publications to date the multifunctionality of these devices have been stressed. The devices have been presented as amplifying filter [3], amplifying switch [4]–[6], [15], amplifying detector [9], etc. Optical bistability in FP SOAs is a well-known phenomenon that may enable the realization of all-optical logic and memory elements [35]–[37]. The short cavity length of VCISOAs and

the possibility of fabricating 2-D arrays are suggested advantages for this application [36]. Optical bistability was recently observed in a reflection-mode VCOSA [37].

VCOSAs may find use in free-space optical interconnects [20]. The attributes of VCOSAs that make them attractive for this application are their circular beam profile, low power consumption, and compatibility with 2-D array architectures. Proposed applications are as modulators, preamplifiers, or buses. As modulators, they are an alternative to MQW electrooptic modulators. Better extinction ratio and low-voltage operation are here foreseen advantages [38]. An array of preamplifiers integrated with a receiver array would ease the requirements on both transmitters and receivers. This would lead to decreased power dissipation, which, in turn, would enable higher interconnect density [20], [39]. The optical bus, or repeater, can serve as detector and amplifier in interconnects between multiple board. Part of the signal is detected and part is passed through to the next board. The amplifier compensates for coupling loss and power absorbed by the detector [40].

Using SOAs for switching/modulation of signals is attractive because of their fast gain dynamics, typically large extinction ratio, and the fact that amplifier gain compensates coupling losses. The gain dynamics enable subnanosecond switching time, which is needed in future all-optical packet-switched systems. The use of in-plane SOAs for switching has been extensively studied [41]–[43]. Limiting factors for in-plane SOAs are polarization dependence and accumulation of ASE as switches are cascaded into switch matrices [43]. The accumulation of ASE can be mitigated by the filtering effect of the narrow VCOSA bandwidth. No multipoint switches based on VCOSAs have yet been demonstrated but the switching properties of individual VCOSA elements have been studied. A vertical-cavity amplifying switch operated in reflection mode at 1.55- μm wavelength has demonstrated a switching time of 10 ps and an extinction ratio of 14 dB [6]. At 1.3 μm , a reflection mode VCOSAs demonstrated similar switching times and 35-dB extinction ratio [15]. The switching properties of transmission mode VCOSAs have not yet been investigated. There have been several reports on VCOSA modulators [38], [44]. Small-signal modulation at 2.5 Gb/s with 5.5-dB fiber-to-fiber gain was reported in [44].

A. Optical Preamplification

Using VCOSAs for optical preamplification might be one of the most interesting applications for these devices. At higher bit rates (10 Gb/s, 40 Gb/s, and beyond) avalanche photodiodes are limited by their gain–bandwidth product. Optical preamplification is a way to increase the sensitivity of a regular p-i-n detector without compromising its high-speed performance. Optical preamplification has been demonstrated using other amplifier technologies (in-plane SOAs [45], EDFAs [46]) but VCOSAs have some clear advantages. Desired properties for this application are good noise performance and polarization-independent gain, which are areas of difficulty for in-plane devices. Also desired are low power consumption, compactness, and low cost, properties that are not associated with fiber amplifiers. VCOSAs can meet all these criteria. Furthermore, an optical filter

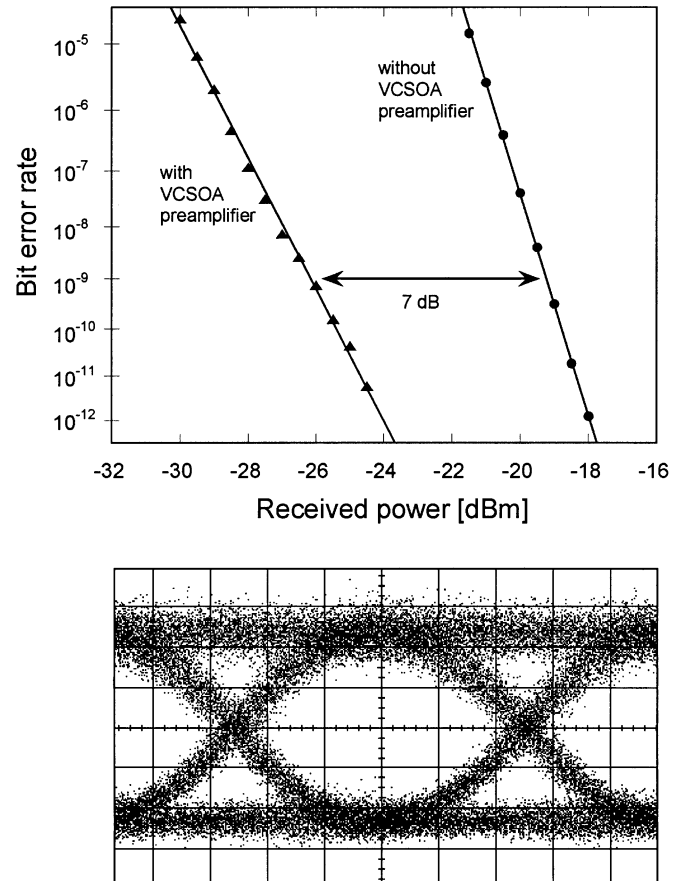


Fig. 13. BER versus received power for VCOSA-preamplified receiver. The eye diagram shows the received preamplified signal at a BER of 10^{-9} .

is normally added after the amplifier for this application, something not needed if VCOSAs are used as their narrow bandwidth makes them function as amplifying filters. The low saturation power of VCOSAs is not a problem for optical preamplification as the signal power reaching the receiver is typically optimized at a lower level than the saturation power of a VCOSA.

We have investigated the feasibility of using our reflection mode VCOSAs for optical preamplification at 10 GB/s. We used a similar setup to the one used for basic VCOSA characterization described above. The input signal was modulated using a 10-Gb/s pattern generator driving a LiNbO₃ Mach–Zehnder modulator. The optically preamplified receiver consisted of the VCOSA, a Nortel PP-10G p-i-n receiver, a dc block, and an electrical broad-band amplifier. The electrical signal from the SHF amplifier was fed to a bit-error rate (BER) tester. No optical filter was used between the VCOSA and the p-i-n detector. The receiver sensitivity was measured with and without the VCOSA preamplifier. A 10-Gb/s nonreturn-to-zero $2^{31} - 1$ pseudorandom bit sequence was transmitted to the receiver and the BER was measured. The BER versus average received optical power is shown in Fig. 13. Without the VCOSA, the receiver sensitivity corresponding to a BER of 10^{-9} was -19.2 dBm. With the VCOSA operating at 11-dB fiber-to-fiber gain, the receiver sensitivity was improved by 7 dB, resulting in a sensitivity of -26.2 dBm. No error floor was observed. The eye pattern at a BER of 10^{-9} is also shown in Fig. 13. Excess noise

from the optical amplification is visible in the high level. The 4-dB power penalty is caused by the high noise figure of the VCSCOA used in the experiment. The device was a planar structure as described above with a top mirror reflectivity of 95.5%. At that reflectivity, the population inversion—and thus noise figure—that could be reached was limited by lasing threshold (the noise figure was estimated to be higher than 10 dB). The gain bandwidth was measured to be 37 GHz. This bandwidth allows for bit rates up to 33 Gb/s. Wider gain bandwidth, which can be achieved by decreasing the pump level or lowering the mirror reflectivity, would allow for transmission at higher bit rates. The carrier-confined VCSCOAs have not yet been used for any transmission experiments, but the receiver sensitivity (for the same p-i-n detector) can be calculated from the measured gain and noise figure of those devices. Using the best results of carrier confined devices, fiber-to-fiber gain of 17 dB and a noise figure of 6.1 dB, a receiver sensitivity at 10 Gb/s of -31 dBm is calculated. For comparison, the best receiver sensitivity reported for an avalanche photodiode (APD) is -28.0 dBm [47].

B. Tunable Amplifiers

As mentioned earlier, the narrow gain bandwidth of VCSCOAs is an advantage for optical preamplification as it eliminates the need for an optical filter before the detector. However, if the signal wavelength is only slightly off from the peak gain wavelength of the VCSCOA distortion of the signal might result. This can be detrimental in any VCSCOA application. Furthermore, the wavelength requirements on sources in low-cost course WDM systems is fairly loose, which has to be accommodated by the amplifiers in the system. It is therefore of great interest to make tunable VCSCOAs that can cover a wider wavelength range and be very precisely adjusted to match the wavelength of the signal. The simplest approach to tune the peak wavelength of a VCSCOA is temperature tuning. In order to be able to maintain constant signal gain when the temperature is increased, the pump power has to be increased to compensate for the decreased gain. Fig. 14 shows the tunability of our planar VCSCOAs. 10 dB of fiber-to-fiber gain over 8-nm tuning range is demonstrated. The input signal power was -30 dBm. To achieve this tuning, the temperature was changed from 15° C to 70° C. The pump power used at each temperature is also shown in Fig. 14. Over 70° C, sufficient gain could not be reached even though the pump power was increased. At temperatures lower than 15° C, it might be possible to expand the tuning range. However, it was not possible to investigate this with the present setup. To achieve a greater tuning range, tunable VCSCOAs could be realized by employing microelectromechanical systems (MEMS), similar to what is being used for tunable VCSELs [29].

One potential path for the future development of VCSCOAs is toward integration with other devices, e.g., VCSELs, detectors, etc. The vertical access and array compatibility are here clear advantages. One example of an interesting possibility for a future device is shown in Fig. 15. It is a tunable VCSCOA integrated with a photodetector. This device takes full advantage of the filtering properties of VCSCOAs and would be very attractive as a tunable, wavelength-selective receiver for application in WDM

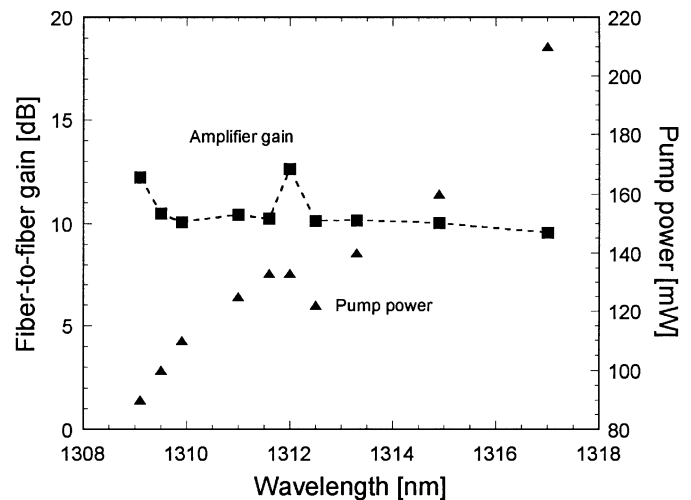


Fig. 14. Temperature tuning of VCSCOA. 10 dB of fiber-to-fiber gain over 8 nm is demonstrated.

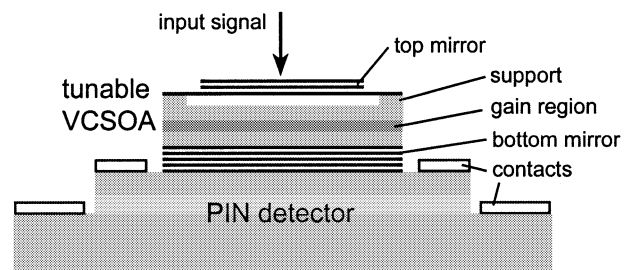


Fig. 15. Schematic of future device. A tunable amplifying filter is monolithically integrated with a detector to form a channel-selective preamplified high-speed receiver.

systems. This could be either single devices or 2-D arrays for parallel applications.

VI. SUMMARY

VCSCOAs are a relatively new class of devices with unique properties. The vertical-cavity geometry gives VCSCOAs a number of advantages over the in-plane design such as polarization-independent gain and a circular-symmetric optical mode; the latter yields high coupling efficiency to optical fiber, which is instrumental in achieving a low noise figure. Compared to conventional in-plane SOAs, they have much lower gain per pass and therefore use feedback provided by mirrors to enhance the signal gain. The balance between the reflectivity of the mirrors and the gain provided by the active region is the central issue in VCSCOA design. The reflectivity of the two mirrors has a large impact on all properties of the amplifier, and must be chosen carefully. The reflectivity should be high enough to provide sufficient feedback so that high amplifier gain can be reached, but low enough so that lasing threshold cannot be reached when the single-pass gain is maximized. This gives the highest possible amplifier gain, the highest saturation power, and the lowest noise figure.

We have designed and fabricated two generations of long-wavelength VCSCOAs. Both generations of devices were optically pumped and operated in reflection mode. Wafer bonding

was used to combine InGaAsP-active material with high-quality AlGaAs DBRs. Wafer bonding gives the opportunity to process the active region of the devices before the structure is completed. This opportunity was used to etch a carrier-confining structure through the active region of the devices. During the second bond, mass transport of InP covered the edges of the QWs, thereby minimizing carrier loss through sidewall recombination. The carrier confinement resulted in a threefold efficiency improvement and an increase in maximum gain compared to planar devices. The results of the carrier-confined devices were 17-dB fiber-to-fiber gain and a noise figure of 6.1 dB.

Optical preamplification at 10 Gb/s was presented in this paper. A VCSEA was operated at 11-dB fiber-to-fiber gain and a bandwidth of 37 GHz. The receiver sensitivity of a p-i-n receiver was improved by 7 dB resulting in a receiver sensitivity of -26.2 dBm. The narrow bandwidth of VCSEAs is a major advantage in this application as out-of-band noise is eliminated, making an additional optical filter redundant. VCSEAs have the advantages of being compatible with low-cost manufacturing techniques and fabrication of 2-D arrays on wafer. The design also lends itself to monolithic integration with, for instance, VCSEL arrays or detector arrays. Tunable VCSEAs can be realized using the same technologies that have been used to make tunable VCSELs. The possibility of realizing arrays of very compact, low-cost devices, which could be tunable and/or integrated with other devices, makes VCSEAs a very promising technology for a wide range of applications in future optical communications systems.

REFERENCES

- [1] M. J. Coupland, K. G. Hambleton, and C. Hilsom, "Measurement of amplification in a GaAs injection laser," *Phys. Lett.*, vol. 7, no. 4, pp. 231–232, Dec. 1963.
- [2] H. Soda, K. Iga, C. Kitahara, and Y. Suematsu, "GaInAsP/InP surface emitting injection lasers," *Jpn. J. Appl. Phys.*, vol. 18, no. 12, pp. 2329–2330, Dec. 1979.
- [3] F. Koyama, S. Kubota, and K. Iga, "GaAlAs/GaAs active filter based on vertical cavity surface emitting laser," *Electron. Lett.*, vol. 27, no. 12, pp. 1093–1095, June 1991.
- [4] R. Raj, J. A. Levenson, J. L. Oudar, and M. Bensoussan, "Vertical microcavity optical amplifying switch," *Electron. Lett.*, vol. 29, no. 2, pp. 167–169, Jan. 1993.
- [5] R. Raj, J. L. Oudar, and M. Bensoussan, "Vertical cavity amplifying photonic switch," *Appl. Phys. Lett.*, vol. 65, no. 18, pp. 2359–2361, Oct. 1994.
- [6] N. Bouché, B. Corbett, R. Kuszelewicz, and R. Ray, "Vertical-cavity amplifying photonic switch at $1.5 \mu\text{m}$," *IEEE Photon. Technol. Lett.*, vol. 8, pp. 1035–1037, Aug. 1996.
- [7] D. Wiedenmann, B. Moeller, R. Michalzik, and K. J. Ebeling, "Performance characteristics of vertical-cavity semiconductor optical amplifiers," *Electron. Lett.*, vol. 32, no. 4, pp. 342–343, Feb. 1996.
- [8] D. Wiedenmann, C. Jung, M. Grabherr, R. Jäger, U. Martin, R. Michalzik, and K. J. Ebeling, "Oxide-confined vertical-cavity semiconductor optical amplifier for 980 nm wavelength," in *CLEO 98 Tech. Dig.*, 1998, Paper CThM5, p. 378.
- [9] R. Lewén, K. Streubel, A. Karlsson, and S. Rapp, "Experimental demonstration of a multifunctional long-wavelength vertical-cavity laser amplifier-detector," *IEEE Photon. Technol. Lett.*, vol. 10, pp. 1067–1069, Aug. 1998.
- [10] E. S. Björilin, B. Riou, A. Keating, P. Abraham, Y.-J. Chiu, J. Piprek, and J. E. Bowers, "1.3- μm vertical-cavity amplifier," *IEEE Photon. Technol. Lett.*, vol. 12, pp. 951–953, Aug. 2000.
- [11] E. S. Björilin, B. Riou, P. Abraham, J. Piprek, Y.-J. Chiu, K. A. Black, A. Keating, and J. E. Bowers, "Long wavelength vertical-cavity semiconductor optical amplifiers," *IEEE J. Quantum Electron.*, vol. 37, pp. 274–281, Feb. 2001.
- [12] E. S. Björilin and J. E. Bowers, "Noise figure of vertical-cavity semiconductor optical amplifiers," *IEEE J. Quantum Electron.*, vol. 38, pp. 61–66, Jan. 2002.
- [13] J. Piprek, S. Björilin, and J. E. Bowers, "Design and analysis of vertical-cavity semiconductor optical amplifiers," *IEEE J. Quantum Electron.*, vol. 37, pp. 127–134, Jan. 2002.
- [14] J. Piprek, E. S. Björilin, and J. E. Bowers, "Optical gain-bandwidth product of vertical-cavity laser amplifiers," *Electron. Lett.*, vol. 37, no. 5, pp. 298–299, Mar. 2001.
- [15] E. S. Björilin, J. Piprek, S. Gee, Y.-J. Chiu, J. E. Bowers, A. Dahl, and P. Abraham, "1.3 μm vertical-cavity amplifying switch," *OSA TOPS Opt. Amplifiers and Their Applications*, vol. 60, pp. 154–160, 2001.
- [16] E. S. Björilin, J. Geske, and J. E. Bowers, "Optically preamplified receiver at 10 Gbit/s using vertical-cavity SOA," *Electron. Lett.*, vol. 37, no. 24, pp. 1474–1475, Nov. 2001.
- [17] E. S. Björilin, P. Abraham, D. Pasquariello, J. Piprek, Y.-J. Chiu, and J. E. Bowers, "High gain, high efficiency vertical-cavity semiconductor optical amplifiers," in *Proc. 14th Indium Phosphide and Related Materials Conf.*, 2002, pp. 307–310.
- [18] C. Tombling, T. Saitoh, and T. Mukai, "Performance predictions for vertical-cavity semiconductor laser amplifiers," *IEEE J. Quantum Electron.*, vol. 30, pp. 2491–2499, Nov. 1994.
- [19] A. Karlsson and M. Höjjer, "Analysis of a VCLAD: Vertical-cavity laser amplifier detector," *IEEE Photon. Technol. Lett.*, vol. 7, pp. 1336–1338, Nov. 1995.
- [20] O. Kibar, "VCSEL-based digital free-space optoelectronic interconnections," Ph.D. dissertation, Dept. Elect. Comput. Eng., Univ. Calif., San Diego, La Jolla, 1999.
- [21] P. Royo, R. Koda, and L. A. Coldren, "Vertical cavity semiconductor optical amplifiers: Comparison of Fabry-Perot and rate equation approaches," *IEEE J. Quantum Electron.*, vol. 38, pp. 279–284, Mar. 2002.
- [22] H. Ghafouri-Shiraz, *Fundamentals of Laser Diode Amplifiers*. West Sussex, U.K.: Wiley, 1996.
- [23] E. S. Björilin, "Long-wavelength vertical-cavity semiconductor optical amplifiers," Ph.D. dissertation, Dept. Elect. Comput. Eng., Univ. Calif., Santa Barbara, 2002.
- [24] T. Mukai, Y. Yamamoto, and T. Kimura, " S/N and error rate performance in AlGaAs semiconductor laser amplifier and linear repeater systems," *IEEE Trans. Microwave Theory Tech.*, vol. MTT-30, pp. 1548–1556, Oct. 1982.
- [25] C. E. Zah, R. Bhat, B. N. Pathak, F. Favire, W. Lin, M. C. Wang, N. C. Andreadakis, D. M. Hwang, M. A. Koza, T. P. Lee, Z. Wang, D. Darby, D. Flanders, and J. J. Hsieh, "High-performance uncooled 1.3- μm Al_xGa_yIn_{1-x-y}As/InP strained-layer quantum-well lasers for subscriber loop applications," *IEEE J. Quantum Electron.*, vol. 30, pp. 511–523, Feb. 1994.
- [26] A. W. Jackson, R. L. Naone, M. J. Dalberth, J. Smith, K. J. Malone, D. W. Kisker, J. F. Klem, K. D. Choquette, D. Serkland, and K. Geib, "OC-48 capable InGaAsN vertical cavity laser," *Electron. Lett.*, vol. 37, no. 6, pp. 355–356, Mar. 2001.
- [27] S. Nakagawa, E. Hall, G. Almuneau, J. K. Kim, D. A. Buell, H. Kroemer, and L. A. Coldren, "1.55- μm InP-lattice-matched VCSEL's with AlGaAsSb-AlAsSb DBRs," *IEEE J. Select. Topics Quantum Electron.*, vol. 7, pp. 224–230, Mar./Apr. 2001.
- [28] V. Jayaraman, T. J. Goodnough, T. L. Beam, F. M. Ahedo, and R. A. Maurice, "Continuous-wave operation of single-transverse-mode 1310-nm VCSEL's up to 115 degrees C," *IEEE Photon. Technol. Lett.*, vol. 12, pp. 1595–1597, Dec. 2000.
- [29] D. Vakhshoori, J.-H. Zhou, M. Jiang, M. Azimi, K. McCallion, C.-C. Lu, K. J. Knopp, J. Cai, P. D. Wang, P. Tayebati, H. Zhu, and P. Chen, "C-band tunable 6 mW vertical-cavity surface-emitting lasers," in *OFC 2000 Tech. Dig. Postconf. Edition*, 2000, Paper PD13, pp. PD13-1–PD13-3.
- [30] A. Black, A. R. Hawkins, N. M. Margalit, D. I. Babic, A. L. Holmes Jr., Y.-L. Chang, P. Abraham, J. E. Bowers, and E. L. Hu, "Wafer fusion: materials issues and device results," *IEEE J. Select. Topics Quantum Electron.*, vol. 3, pp. 943–951, June 1997.
- [31] L. A. Coldren and S. W. Corzine, *Diode Lasers and Photonic Integrated Circuits*. New York: Wiley, 1995.
- [32] E. Yablonoitch, C. J. Sandroff, R. Bhat, and T. Gmitter, "Effects of passivating ionic films on the photoluminescence properties of GaAs," *Appl. Phys. Lett.*, vol. 51, no. 24, pp. 2022–2024, Dec. 1987.
- [33] J. J. Hsieh and C. C. Shen, "Room-temperature CW operation of buried-stripe double-heterostructure GaInAsP/InP diode lasers," *Appl. Phys. Lett.*, vol. 30, no. 8, pp. 429–431, Apr. 1977.
- [34] Z.-L. Liao and J. N. Walpole, "Mass-transported GaInAsP/InP lasers," *Lincoln Lab. J.*, vol. 2, no. 1, pp. 77–94, 1989.

- [35] D. A. H. Mace, M. J. Adams, and C. Seltzer, "MQW amplifier optical bistability," *Electron. Lett.*, vol. 27, no. 15, pp. 1363–1365, July 1991.
- [36] P. Pakdeevanich and M. J. Adams, "Measurements and modeling of reflective bistability in 1.55- μm laser diode amplifiers," *IEEE J. Quantum Electron.*, vol. 35, pp. 1894–1903, Dec. 1999.
- [37] P. Wen, M. Sanchez, M. Matthias Gross, and S. Esener, "Observation of bistability in a vertical-cavity semiconductor optical amplifier (VCSOA)," *Opt. Express*, vol. 10, no. 22, pp. 1273–1278, Nov. 2002.
- [38] P. Wen, M. Sanchez, O. Kibar, and S. C. Esener, "Low-voltage, high contrast-ratio, low-noise VCSEL modulator," in *Proc. OSA Topical Meet. Optical Amplifiers and Their Applications*, 2000, pp. 265–266.
- [39] O. Kibar, P. J. Marchand, and S. C. Esener, "Gain-bandwidth product of a VCSEL amplifier," in *Proc. LEOS 11th Annu. Meet.*, 1998, pp. 221–222.
- [40] N. Suzuki, M. Ohashi, and M. Nakamura, "A proposed vertical-cavity optical repeater for optical inter-board connections," *IEEE Photon. Technol. Lett.*, vol. 9, pp. 1149–1151, Aug. 1997.
- [41] M. Ikeda, "Switching characteristics of laser diode switch," *IEEE J. Quantum Electron.*, vol. QE-19, pp. 157–164, Feb. 1983.
- [42] M. Gustavsson, B. Lagerström, L. Thylén, M. Janson, L. Lundgren, A.-C. Mörner, M. Rask, and B. Stolz, "Monolithically integrated 4×4 InGaAsP/InP laser amplifier gate switch arrays," *Electron. Lett.*, vol. 28, no. 24, pp. 2223–2225, Nov. 1992.
- [43] E. Almström, C. P. Larsen, L. Gillner, W. H. van Berlo, M. Gustavsson, and E. Berglind, "Experimental and analytical evaluation of packaged 4×4 InGaAsP/InP semiconductor optical amplifier gate switch matrices for optical networks," *J. Lightwave Technol.*, vol. 14, pp. 996–1004, June 1996.
- [44] E. S. Björilin, A. Dahl, J. Piprek, P. Abraham, Y.-J. Chiu, and J. E. Bowers, "Vertical-cavity amplifying modulator at 1.3- μm ," *IEEE Photon. Technol. Lett.*, vol. 13, pp. 1271–1273, Dec. 2001.
- [45] T. Ducellier, R. Basset, J. Y. Emery, F. Pommereau, R. N'Go, J. L. Lafragette, P. Aubert, P. Doussière, P. Laube, and L. Goldstein, "Record low noise factor (5.2 dB) in 1.55 mm bulk SOA for high bit rate low-noise preamplification," in *Tech. Dig. ECOC'96*, vol. 3, 1996, pp. 173–176.
- [46] R. I. Laming, A. H. Gnauck, C. R. Giles, M. N. Zervas, and D. N. Payne, "High-sensitivity two-stage erbium-doped fiber preamplifier at 10 Gb/s," *IEEE Photon. Technol. Lett.*, vol. 4, pp. 1348–1350, Dec. 1992.
- [47] K. Sato, T. Hosoda, Y. Watanabe, S. Wada, Y. Iriguchi, K. Makita, A. Shono, J. Shimizu, K. Sakamoto, I. Watanabe, K. Mitamura, and M. Yamaguchi, "Record highest sensitivity of -28.0 dBm at 10 Gb/s achieved by newly developed extremely-compact superlattice-APD modulae with TIA-IC," in *Tech. Dig. 27th Optical Fiber Communication Conf. (OFC '02), Postdeadline Papers*, Mar. 2002, pp. FB11-1–FB11-3.



E. Staffan Björilin (M'02) received the M.S. degree in engineering physics from the Royal Institute of Technology (KTH), Stockholm, Sweden, in 2000, and the Ph.D. degree in electrical engineering from the University of California, Santa Barbara, in 2002.

He is currently a Postdoctoral Researcher with Prof. J. E. Bowers at the University of California, Santa Barbara. His current research interests include the design and analysis of long-wavelength vertical-cavity semiconductor optical amplifiers.



Toshio Kimura received the B.S. degree in physics from Keio University, Keio, Japan, in 1993 and the M.S. degree in electrical engineering from Tokyo Institute of Technology, Tokyo, Japan, in 1995.

Since 1995, he has been employed by Furukawa Electric Co., Ltd., Japan where he worked on high-power pump sources for EDFAs. He joined Prof. J. E. Bowers's group at the University of California, Santa Barbara, in May 2002. His interests include vertical cavity semiconductor optical amplifiers.



John E. Bowers (F'93) received the M.S. and Ph.D. degrees from Stanford University, Stanford, CA.

He is Director of the Multidisciplinary Optical Switching Technology Center (MOST), and a Professor in the Department of Electrical Engineering at the University of California, Santa Barbara (UCSB). His research interests are primarily concerned with optoelectronic devices and optical networking. He is cofounder of the Center for Entrepreneurship and Engineering Management, a founder of Terabit Technology, and Calient Networks. He has worked for AT&T Bell Laboratories and Honeywell before joining UCSB. He has published six book chapters, over 250 journal papers, over 250 conference papers, and has received 26 patents.

Dr. Bowers is a Fellow of OSA and the American Physical Society, and a recipient of the IEEE LEOS William Streifer Award. He serves on the Board of Directors of Calient Networks.